Elsevier Editorial System(tm) for Applied Mathematics and Computation

Manuscript Draft

Corresponding Author: Mr. Badr Mohammed Lahasan, MSc

Corresponding Author's Institution: Universiti Sains Malaysia (USM)

First Author: Badr Mohammed Lahasan, MSc

Order of Authors: Badr Mohammed Lahasan, MSc; Ibrahim Venkat; Mohammed Al-Betar; Syheerah Lutfi; Philippe De Wilde

Abstract: An intuitive graph optimization face recognition approach called Harmony Search Oriented-EBGM (HSO-EBGM) inspired by the classical Elastic Bunch Graph Matching (EBGM) graphical model is proposed in this contribution. In the proposed HSO-EBGM, a recent evolutionary approach called harmony search optimization is tailored to automatically determine optimal facial landmarks. A novel notion of face subgraphs have been formulated with the aid of these automated landmarks that maximizes the similarity entailed by the subgraphs. For experimental evaluation, two sets of de facto databases (i.e., AR and Face Recognition Grand Challenge (FRGC) ver2.0) are used to validate and analyse the behavior of the proposed
HSO-EBGM in terms of number of subgraphs, varying occlusion sizes, face images under controlled /ideal
conditions, realistic partial occlusions, expression variations and varying illumination conditions. For a number of experiments, results justify that the HSO-EBGM shows improved recognition performance when compared to recent state-of-the-art face recognition approaches.

Cover Letter

Dear Editor

We are pleased to submit our paper titled "***Recognizing faces prone to occlusions and common variations using optimal face subgraphs***" for the consideration of publication in the Journal of Applied Mathematics and Computation.

We have formulated several novel notions and taken efforts to illustrate these notions via several useful diagrams. We believe that our findings in this paper would be beneficial to the readers of both the domains viz.: optimization and face recognition.

Thanks and warm regards

Sincerely

Badr Mohammed Lahasan
School of Computer Sciences
Universiti Sains Malaysia (USM)
Penang, Malaysia.

Recognizing faces prone to occlusions and common variations using optimal face subgraphs

Badr Mohammed Lahasan[a,*], Ibrahim Venkat[a], Mohammed Azmi Al-Betar[b], Syaheerah Lebai Lutfi[a],
Philippe De Wilde[c]

[a]*School of Computer Sciences, Universiti Sains Malaysia, 11800 USM, Malaysia*
[b]*Department of Information Technology, Al-Huson University College, Al-Balqa Applied University, Jordan*
[c]*University of Kent, Canterbury, UK*

Abstract

An intuitive graph optimization face recognition approach called Harmony Search Oriented-EBGM (HSO-EBGM) inspired by the classical Elastic Bunch Graph Matching (EBGM) graphical model is proposed in this contribution. In the proposed HSO-EBGM, a recent evolutionary approach called harmony search optimization is tailored to automatically determine optimal facial landmarks. A novel notion of face subgraphs have been formulated with the aid of these automated landmarks that maximizes the similarity entailed by the subgraphs. For experimental evaluation, two sets of *de facto* databases (i.e., AR and Face Recognition Grand Challenge (FRGC) ver2.0) are used to validate and analyse the behavior of the proposed HSO-EBGM in terms of number of subgraphs, varying occlusion sizes, face images under controlled /ideal conditions, realistic partial occlusions, expression variations and varying illumination conditions. For a number of experiments, results justify that the HSO-EBGM shows improved recognition performance when compared to recent state-of-the-art face recognition approaches.

Keywords: Harmony Search, Face recognition, Occlusion, Optimization, Graphical model.

1. INTRODUCTION

Automatic face recognition has been a subject of intensive research for the past few decades. It is the problem of recognizing humans by matching a given face with face images stored in a database. As an interest, it is a challenging task where the performance of a typical face recognition algorithm usually degrades considerably due to several variations such as expressions, illumination conditions and facial occlusions [32, 15]. Therefore, developing a robust face recognition system amidst these variations is still an open research area as stated in recent studies [45, 12, 1, 17]. Face recognitions systems have an essential role in biometric-oriented video surveillance systems which have been progressively incorporated in operational environments where the problem of encountering occlusions cannot be avoided. [38].

Several approaches have been proposed to overcome the shortcomings of face recognition challenges: expressions, illumination conditions and facial occlusions [30, 41, 16, 42, 28, 44, 38]. In general, occluded face recognition approaches are classified into two categorizes: holistic and component-based. Holistic category manipulates the face image as a whole entity. In contrast, component-based category deals with occlusions by matching local regions rather than matching the whole entity [10]. Furthermore, in component-based approaches, the face image is partitioned into various segments and each segment is tackled independently. These models deal with occlusion by detecting the occluded areas then the results are manipulated by either reconstructing or discarding these areas. Notably, it has been observed that the reconstruction approaches

---

[*]Corresponding author at: School of Computer Sciences, Universiti Sains Malaysia, 11800 USM, Penang, Malaysia.
E-mail address: bmo12_com009@student.usm.my (B.M. Lahasan), Tel: +604-6534753, Fax: +604-6573335

such as [23, 24, 14] are not effective in the presence of large occlusions because the identity information can be contaminated during in-painting [39]. Omitting occluded areas in the face recognition might lead to loss of information but considering these areas might be discriminative and could increase the overall recognition rate.

Among the face recognition approaches which are holistic in nature, the Elastic Bunch Graph Matching (EBGM) is one of the most successful graph-based technique [40, 11, 36]. EBGM has been successfully applied for a wide range of face recognition problems [34]. However, it suffers from a major drawback whereby manual landmark selection is required in the initial stage of the recognition process. The automation-based systems require the modern face recognition systems to be totally automatic without the need to any intervention from the human side; for example the manual selection of the facial landmarks. One of the focus point of this study is to reformulate the EBGM as an optimization problem with the aid of Harmony Search (HS) so as to compute optimal facial landmarks in an automatic way.

Human faces have useful facial landmarks that possess various information. Furthermore, psychological studies in face recognition [37] demonstrate that some facial landmarks are distinguished and more beneficial than others in terms of recognition accuracy. Thus, finding the optimal facial landmarks from the whole face image is required for efficient recognition. To cope with these issues, the meta-heuristic search techniques are most suitable to automatically determine the optimal facial landmarks.

Harmony search algorithm (HSA) is a recent meta-heuristic algorithm inspired from the music improvisation process [21]. It has several advantages over other metaheuristic-based approaches due to its derivative-free characteristics [20]. Therefore, HSA has been successfully tailored for a wide range of optimization problems such as timetabling [5, 7, 6], bio-informatics [3], image enhancements [9], scheduling problem of multiple dam system [19] and structural optimization [27] and many others as reported in [8, 29]. In the face recognition domain, HSA was primarily used for feature selection problems [25, 35] where using HSA on feature selection has shown improvements in terms of recognition accuracy.

In this study, a transformed image recognition approach is proposed based on HSA and component-based EBGM. This method is abbreviated as *Harmony Search Oriented - EBGM (HSO-EBGM)* which is able to automatically determine the optimal facial landmarks using HS. These potential landmarks serve as inputs for the modified EBGM face recognition approach which intends to recognize faces prone to several challenges such as occlusions, varying illumination conditions and facial expressions. The proposed component-based EBGM enables the model to tackle these challenges without demanding any prior knowledge or assumption about the occluded regions in the targeted face image. Interestingly, the component-based mechanism deployed in the proposed HSO-EBGM for handling partial occlusions neither discard any occluded region from similarity calculation, nor reconstruct this occluded region.

The effectiveness of the proposed HSO-EBGM method is evaluated using the AR [31] and Face Recognition Grand Challenge (FRGC ver2.0) [33] databases. The experimental results have shown that the proposed HSO-EBGM method can improve the accuracy of recognizing faces prone to occlusion and other variations such as expression and illumination. For comparative evaluation, the performance of the proposed HSO-EBGM is compared against the standard EBGM [11] and another five state-of-the-art-methods including Psychophysically Inspired Similarity MApping (PISMA) [38], Line Edge Map (LEM) [18], Ensemble String Matching (ESM) [13], Adaptively Weighted Sub-Gabor Array (AWSGA) [23], and Adaptively Weighted Patch Pseudo Zernike Moment Array (AWPPZMA) [24] using AR and FRGC ver2.0. The comparative results show that the proposed methods excels the comparative methods in almost all cases.

This article is organized as follows: Section 2 provides a description of the Elastic Bunch Graph Matching (EBGM) . The formulation of the facial occlusions problem is presented in Section 3. In Section 4 the proposed method is illustrated. Next, Section 5 reports the experimental results and discussions on the findings. Finally, we conclude the work and briefly suggest future research directions in Section 6.

2. Elastic Bunch Graph Matching (EBGM)

Elastic Bunch Graph Matching (EBGM) algorithm presented by Bolme (2003) is one of the mainstream face recognition algorithms [11]. In the initial stage of the EBGM implementation, sample set of images

have to be chosen referred as model images. These images should account for different face image variations such as variations due to gender, race, and age; in addition to faces with open eyes, closed eyes, sunglasses and so on. Then, for each image, facial landmark points such as eyes, mouth and nose are chosen manually. Thereafter, The Gabor wavelets transform are extracted for each manually selected landmark and named as a jet (as shown in Fig. 2). The jets that were extracted from the model images are called model jets. Model jets are gathered in a data structure called Face Bunch Graph (FBG) as shown in Figure 3. Each node of the bunch graph contains a set of M jets where M is the number of model images (70 image were used [11]). One of the advantages of modeling a bunch graph is that there are different instances of landmarks that are stored in the corresponding bunches. For example model jets of eyes with glasses, eyes that are closed/opened and eyes under different lighting are available. Furthermore, the jets from different individuals for each landmark on the face were provided. The FBG is used for landmarks localization in the novel image where the node positions on the new image is estimated using the average values of node positions of the FBG. The node positions are refined by calculating the similarity between jets from estimation positions and the corresponding jets of the FBG where the maximum jet similarities represent the location of the nodes. In more details,the facial landmark points for a given new face image are found by by comparing the new face image against the FBG and finding the landmark points with the highest similarity. A detailed method is available in [11]. The basic idea is summarized as follow: The initial position of a new node is estimated by calculating the average distance between the previously located node on the FBG. For example the location of the nose bridge can be estimated by using the eye coordinates and then this location can be further refined by comparing the Gabor jet extracted from the estimated point to a model jet from the bunch graph. Once the location of the three landmarks (eyes and nose bridge) are known, the location of the eyebrow can easily be estimated. The corresponding jet is extracted from the estimated location of the new image node. The similarity with each jet in the FBG is calculated for that node. The goal is to maximize the similarity with the FBG in a neighborhood. Finally, the coordinates where the maximum similarity has been obtained are saved. This procedure is iterated for the remaining nodes of the graph. Then based on those landmarks and their jets, the face graph of any novel image (probe face) is constructed. A typical face graph includes twenty five landmarks encompassed by edges (see Fig.1) and they are located around the eyes, nose, mouth and the edge of the face. When the face graph of the novel image is obtained, the matching process between face graph of the probe face image and the face graphs of the reference images which are readily stored in the database is performed in order to recognize the probe face image.

The basic steps involved in the EBGM algorithm [11] are as follows:

Step 1 : Initially, facial landmarks are selected manually (as in Fig. 2) and their corresponding jets (Js) are extracted .

Step 2 : Create the bunch graph by collecting all the model jets extracted from the model images and store them in bunches (Bs). Each bunch contains nodes that correspond to the facial landmarks on the model images (as in Fig. 3).(i.e., the right eyes of the all model images $(J_{11}, J_{12}, \cdots)$ Fig (2) are collected in bunch one ,the left eyes $(J_{12}, J_{22}, \cdots)$ on bunch two and so on as illustrated on Fig 3)

Step 3 : Locate the landmarks for each new face image. Next, new jets are extracted from the new image. Then, by comparing each jet to the most similar model jet from the corresponding bunch, the location of the jets are adjusted based on displacements computed from actual locations.

Step 4 : Create face graph for each face. The face graph contains the locations of each landmarks and its jet values . The original image can then be discarded.

Step 5 : Ultimately face similarity is computed as a function of landmarks and jet values.

3. Formulation of the objective function for face recognition

In simple terms, facial occlusion refers to the masking of face images by sunglasses, hair, veils, wrapping the faces by hand or with any accessories. In order to recognize an occluded face by matching it with face images stored in the database (reference images), initially a subset of landmarks need to be determined to represent the face image [11, 40]. For the purpose of this paper, the face image is segmented into k segments

$(k_1, k_2, \cdots, k_{2r})$, where r is the number of horizontal segments as shown in Fig (4a). The idea is to represent each segment as a face subgraph, instead of treating each face as a whole face graph as used in the standard EBGM.

For each segment k_i, the aim is to find the optimal landmark positions (x-axes and y-axes image pixel coordinates) which is represented by a vector $\boldsymbol{x} = (x_1, x_2 \cdots x_M)$ where each x_i owns a specific value range $[LB_i, UB_i]$. Note that LB_i represents the lower bound and UB_i represents the upper bound for x_i.

Each segment k_i is divided into M portions along the x-axis (p_x)and M portions along the y-axis (p_y) where the range of each element of x is determined by the range $[LB_i, UB_i]$. An illustration of generation of landmarks for a typical face segment is shown in Fig 5 which is further explained as follows: Let the vector $\boldsymbol{x} = (x_1, x_2, x_3, x_4)$ represents a segment k_1 of size 40×40 pixels. The segment k_1 is divided into four portions along with x-axis and four portions along with y-axis. Therefore the search range of the first variable x_1 of vector $\boldsymbol{x}$ will be selected from a value range of $[LB_1 = 1, UB_1 = 10]$; $x_2 \in [LB_2 = 11, UB_2 = 20]$,$x_3 \in [LB_3 = 21, UB_3 = 30]$, and $x_4 \in [LB_4 = 31, UB_4 = 40]$.

According to the concept of permutation and combination, the set of all possible landmarks in each facial segment k_i is represented by M^2 as shown in Fig (4 b), where the landmark coordinates (LC) are generated from the vector $\boldsymbol{x}$ as follows:

$$LC = \begin{pmatrix} (x_1, x_1) & (x_1, x_2) & \cdots & (x_1, x_M) \\ (x_2, x_1) & (x_2, x_2) & \cdots & (x_2, x_M) \\ \vdots & \vdots & \vdots & \vdots \\ (x_M, x_1) & (x_M, x_2) & \cdots & (x_M, x_M) \end{pmatrix} \tag{1}$$

where LC matrix elements represent the corresponding landmark points inside a particular image segment. For example the element (x_1, x_1) is a point of the first landmark shown in Fig. 4b.

For each landmark point in the LC matrix, the Gabor wavelet transform is computed with F_r frequencies indexed as $v = (0, ..., F_r - 1)$ and O_r orientations indexed as $\mu = (0, 1, ..., O_r - 1)$. In the literature, the values of $F_r = 5$ and $O_r = 8$ is recommended [11, 2, 43]. Then, a total of $F_r \times O_r$ complex coefficients is generated for each landmark. The vector J of the length $F_r \times O_r$ coefficients is calculated for each landmark point in LC which is referred to as a Jet.

A Jet J describes a small patch of grey values in an image I($\overrightarrow{x}$) around a given input pixel $\overrightarrow{x} = (x_{p_x}, x_{p_y})$. It is based on a wavelet transform, defined as a convolution shown below [40]: $\forall j \in I$,

$$\Psi_j(\overrightarrow{x}) = \int I(\overrightarrow{x'}) \psi_j(\overrightarrow{x} - \overrightarrow{x'}) d^2\overrightarrow{x'} \tag{2}$$

with Gabor-based kernels :

$$\psi_j(\overrightarrow{x}) = \frac{\|\overrightarrow{K_j}\|^2}{\sigma^2} e^{\frac{\|\overrightarrow{K_j}\|^2 \|\overrightarrow{x}\|^2}{2\sigma^2}} [e^{i\overrightarrow{K_j}\overrightarrow{x}} - e^{\frac{-\sigma^2}{2}}] \tag{3}$$

the wave vector $\overrightarrow{K_j}$ describes different frequencies (v) and orientations (μ) enveloped by a Gaussian function, where $\sigma = 2\pi$ is the standard deviation of this Gaussian, $\overrightarrow{x} = (x_{p_x}, x_{p_y})$ represents landmark location in LC matrix. The values of $\overrightarrow{K_j}$ is defined as:

$$\overrightarrow{K_j} = \begin{pmatrix} K_{x_{p_x}} \\ K_{x_{p_y}} \end{pmatrix} = \begin{pmatrix} K_v \cos \theta_\mu \\ K_v \sin \theta_\mu \end{pmatrix} \tag{4}$$

where:

$$K_v = \frac{k_{max}}{f^v} \tag{5}$$

$$\theta_\mu = \mu \frac{\pi}{8} \tag{6}$$

For the purpose of our implementation, f is chosen to be $\sqrt{7}$ and $k_{max} = \frac{\pi}{2}$ as suggested in [26].

4

As aforementioned, the length of a Jet vector J has $F_r \times O_r$ complex coefficients $J = (a_1, a_2, \cdots, a_{F_r \times O_r})$. Therefore, the $\boldsymbol{J}$ vector could be represented by a total of $F_r \times O_r$ magnitude values $(|a_1|, |a_2|, \cdots, |a_{F_r \times O_r}|)$ and total of $F_r \times O_r$ phase θ $(\theta_1, \theta_2, \cdots, \theta_{F_r \times O_r})$. The θ values can be defined as follows:

$$
\theta = \begin{cases} arctan(a_{imag}/a_{real}) & \text{if } a_{real} > 0 \\ \pi + arctan(a_{imag}/a_{real}) & \text{if } a_{real} < 0 \\ \pi/2 & \text{if } a_{real} > 0 \quad \text{and } a_{imag} \geq 0 \\ -\pi/2 & \text{if } a_{real} > 0 \quad \text{and } a_{imag} < 0 \end{cases} \tag{7}
$$

The similarity of the landmark points of two correspondent segments in two different images are calculated based on the their Jet vectors. Let $\boldsymbol{J}$ and $\boldsymbol{J}'$ represent the jet vectors formed by the landmark points of corresponding facial segments of model and reference face images respectively. Model images of a subject comprise of image variations viz., occlusion (sunglasses and scarf), expression and illumination which are used to generate the average landmark locations. Whereas, the *reference image* is the neutral image available in the face database that used for matching a given probe image.

Our objective is to find the optimal landmarks possessed in the facial segments that maximize the similarity between the corresponding $\boldsymbol{J}$ and $\boldsymbol{J}'$. Thus, the objective function can be defined as follows: $\forall j \in \boldsymbol{J}, \boldsymbol{J}'$

$$
f(\boldsymbol{x}) = \max S(\boldsymbol{J}, \boldsymbol{J}') \tag{8}
$$

$$
S(\boldsymbol{J}, \boldsymbol{J}') = \frac{\sum_j |a_j||a_j'|cos(\theta_j - \theta_j')}{\sqrt{\sum_j |a_j|^2 \sum_j |a_j|^2}} \tag{9}
$$

4. The proposed methodology

In this section, we present the proposed methodology of HSO-EBGM which can be divided into five consecutive stages as shown in Fig. 6.

In stage one, the image information are retrieved from the image database. Then, all the images are enhanced by Median Filtering and Histogram Equalization techniques to remove the noise and enhance the contrast levels. In this stage also, there are two types of images for each subject: one natural image (i.e., reference image) and four images with other variations (i.e., modal images). Thereafter, in stage 2, each face image is portioned into six separable segments which will be illustrated in Sec. 4.1. For the next stage, the harmony search algorithm is used to find the optimal landmark points for each segments of all face images. This stage is thoroughly discussed in Sec. 4.2. In stage 4, based on the optimal landmarks obtained by harmony search, the face subgraph of each face image segment is constructed after the landmarks located in the background image are eliminated. In the final stage, the test (probe) face image is recognized based on the average positions (location) of the sub-graph nodes previously constructed.

These main stages of the proposed HSO-EBGM approach are described with more details in the following subsections:

4.1. Face image segmentation

Each face image has been segmented into r horizontal segments. These r segments are further subdivided into two vertical segments, one for the left half and the other for the right half of the face image thereby yielding $k = 2 \times r$ segments. The idea is to represent each segment as a face sub-graph, instead of treating each face as one whole face-subgraph as used by the standard EBGM described in Sec.1. Figure 7 shows a typical face and its segmented components for the case of $r = 3$. The formulation of face sub-graphs are carried out as follows:

Let $I(x, y)$ be a given face whose height and width are represented as H and W respectively. Let $I(x_0, y_0)$ represent the coordinates of its upper left point. We can use the set theory notation [22] to model the facial components (segments) as follows:

The left-half components $k_1, k_3, \cdots, k_{2r-1}$ can be modeled as:

$$
\begin{aligned}
k_1(I(x,y)) &= \{(x,y) \mid x_0 \le x \le x_0 + \frac{W}{2}, y_0 \le y \le y_0 + \frac{H}{r}\} \\
k_3(I(x,y)) &= \{(x,y) \mid x_0 \le x \le x_0 + \frac{W}{2}, y_0 + \frac{H}{r} \le y \le y_0 + \frac{2H}{r}\} \\
&\vdots \\
k_{2r-1}(I(x,y)) &= \{(x,y) \mid x_0 \le x \le x_0 + \frac{W}{2}, y_0 + \frac{2H}{r} \le y \le y_0 + H\}
\end{aligned}
\tag{10}
$$

Similarly the right-half facial components $k_2, k_4, \cdots, k_{2r}$ can be modeled as:

$$
\begin{aligned}
k_2(I(x,y)) &= \{(x,y) \mid x_0 + \frac{W}{2} < x \le x_0 + W, y_0 \le y \le y_0 + \frac{H}{r}\} \\
k_4(I(x,y)) &= \{(x,y) \mid x_0 + \frac{W}{2} < x \le x_0 + W, y_0 + \frac{H}{r} < y \le y_0 + \frac{2H}{r}\} \\
&\vdots \\
k_{2r}(I(x,y)) &= \{(x,y) \mid x_0 + \frac{W}{2} < x \le x_0 + W, y_0 + \frac{2H}{r} < y \le y_0 + H\}
\end{aligned}
\tag{11}
$$

4.2. Determination of the landmark positions by harmony search

For each image segment, the Harmony Search (HS) algorithm will be invoked to determine its optimal landmark positions. As stated in the literature some facial landmarks are more discriminatory than others. Therefore selecting these discriminatory landmarks will play a key role in the matching process between given two face images which will eventually improve the recognition accuracy [37].

The harmony search algorithm has five main steps which are shown in the flowchart represented in Fig.8. These steps are described as follows:

Step 1: *Initialize the face recognition problem and harmony search parameters*. In section 3, the modeling of the objective function $f(\boldsymbol{x})$ is formulated in eq. (8). The solution is represented as a vector $\boldsymbol{x} = (x_1, x_2, \ldots, x_M)$ of landmark positions. The value range of each landmark position $x_i \in [LB_i, UB_i]$ is also provided. The following parameters of HS required to solve the face recognition problem have to be specified in this step:

 i Harmony Memory Size (HMS) determines the number of facial vectors in the Harmony Memory(HM).
 ii Harmony Memory Considering Rate (HMCR) which determines whether the value of a landmark position is selected from the accumulative search or randomly from its possible range.
 iii Pitch Adjustment Rate (PAR) is determined to adjust the value of the new landmark position selected from memory by a small value.
 iv The distance bandwidth (BW) determines the distance of adjustment in the pitch adjustment operator.
 v Maximum Number of Iterations (NI).

Step 2: *Initialize the Harmony Memory (HM)* . For each segment of the image, facial vectors are randomly generated as many as HMS. i.e., $x_i^j = LB_i + (UB_i - LB_i) \times U(0,1)$, $\forall i = 1, 2, \ldots, M$ and $\forall j = 1, 2, \ldots, \text{HMS}$ where $U(0,1)$ generate a uniform random number between 0 and 1. They will be also arranged in descending order according to their objective function values as shown in Eq. 12.

$$\mathbf{HM} = \begin{bmatrix} x_1^1 & x_2^1 & \cdots & x_M^1 \\ x_1^2 & x_2^2 & \cdots & x_M^2 \\ \vdots & \vdots & \cdots & \vdots \\ x_1^{HMS} & x_2^{HMS} & \cdots & x_M^{HMS} \end{bmatrix}. \tag{12}$$

Step 3: *Improvise a new harmony.*

In this step, the HS algorithm generates (improvise) a new harmony vector (or new facial occlusion vector) from scratch, $\boldsymbol{x}' = (x_1', x_2', \cdots, x_M')$, based on three operators: (*i*) memory consideration, (*ii*) pitch adjustment and (*iii*) random consideration.

Memory consideration. In memory consideration, the value of the first landmark position x_1' is randomly *selected* from the historical landmark positions , $\{x_1^1, x_1^2, \ldots, x_1^{HMS}\}$, stored in HM vectors. Values of the other landmark positions, $(x_2', x_3', \ldots, x_N')$, are sequentially selected in the same manner with probability (w.p.) HMCR $\in (0,1)$.

Pitch adjustment. Each landmark position x_i' of a new harmony vector, $\boldsymbol{x}' = (x_1', x_2', x_3', \ldots, x_M')$, that has been assigned a value by memory considerations is pitch adjusted with the a probability of PAR where PAR $\in (0,1)$ as follows:

$$\text{Pitch adjusting decision for } x_i' \leftarrow \begin{cases} \text{Yes} & \text{w.p.} & \text{PAR} \\ \text{No} & \text{w.p.} & \text{1-PAR.} \end{cases}$$

If the pitch adjustment decision for x_i' is Yes, the value of x_i' is adjusted to its neighboring value as follows: $x_i' = x_i' \pm U(0,1) \times BW$, where BW is

Random consideration. Landmark positions that are not assigned with values according to memory consideration are randomly assigned according to their possible range by random consideration with a probability of (1-HMCR) as follows:

$$x_i' \leftarrow \begin{cases} x_i' \in \{x_i^1, x_i^2, \ldots, x_i^{HMS}\} & \text{w.p.} & \text{HMCR} \\ x_i' \in [LB_i, UB_i] & \text{w.p.} & \text{1 - HMCR.} \end{cases}$$

Step 4: *Update harmony memory.* If the new harmony vector, $\boldsymbol{x}' = (x_1', x_2', \cdots, x_M')$, is better than the worst harmony $\boldsymbol{x}^{\text{worst}}$ stored in HM in terms of the objective function value (i.e., $\boldsymbol{x}^{\text{worst}} = \boldsymbol{x}^{\text{HMS}}$ in case HM is sorted), the new harmony vector is included to the HM, and the worst harmony vector is excluded from the HM.

Step 5: *Stopping Criterion.* In Step 5, the HS algorithm will repeat Step 3 and Step 4 until the maximum number of iterations specified by NI parameter is reached.

4.3. Construction of face sub-graphs

After the optimal landmark is found by the HS algorithm for each segment in both reference and model images, some constraints that relies on the pixel intensity variation information of the face image segment and the landmark distance from the center of face segment are applied especially for k_{r-1}, k_r (because they contain parts of image background) to ensure that all landmarks are located within the face image. These constraints are eliminated as follows:

let $\Omega = P(x, y)$ be a landmark, and ψ represent an eligible landmark so that :

$$\Omega \in \psi \text{ if} \begin{cases} \Omega \neq 255 \text{ or } 0 \\ \\ \rho \geq \tau \end{cases} \tag{13}$$

7

where ρ is the pixel intensity variance and calculated as:

$$\rho = \|\Omega - U\| \tag{14}$$

$$U = \frac{1}{P \times Q} \sum_{x-1}^{P} \sum_{y=1}^{Q} P(x,y) \tag{15}$$

and τ is a threshold (empirically $\tau = 140$ yields good results), P and Q are the dimensions of the segment.

The validation scheme is illustrated in Figure (9). Fig. (9b) shows that after validation, facial landmarks that are not located within the face (Fig. 9a) are successfully eliminated.

A face subgraph is constructed for each segment k_i of the model images using the optimal landmarks found by HS algorithm which exhibits the maximum similarity between each face subgraph of the corresponding reference images. Each optimal facial solution $\boldsymbol{x} = (x_1, x_2, \ldots, x_M)$ is used to generate the subgraph of each segment. The solution $\boldsymbol{x}$ is mapped into LC matrix shown in eq.(1) where each point in LC is a node in the subgraph. The edges between the adjacent nodes are fully connected. Furthermore, the Jet vector of each node is calculated as discussed in eq. (3).

Now, the proposed model is ready for the recognition process. The probe image (which is the test face to be recognize) also need to be segmented. Thereafter, the the average landmark positions stored in a AVG_{k_i} matrix for the corresponding segments k_i in all modal images using their LC matrix is calculated as follows:

$$AVG_{k_i} = \frac{1}{N_m} \sum_{t=1}^{N_m} LC_t, \tag{16}$$

where N_m is the number of model images (in this study N_m=4). The AVG_{k_i} is used to construct the face subgraphs for the probe image. In simple terms, the size of AVG_{k_i} matrix of each segment k_i is equal to the size of its LC where each element in AVG_{k_i} is the average of corresponding elements in the LC from all model images. For example suppose that the following information are in LC_{k_1} :

- $LC_1(x_1, x_1)$ from k_1 of model image 1 = (3,3);

- $LC_2(x_1, x_1)$ from k_1 of model image 2 = (7,7);

- $LC_3(x_1, x_1)$ from k_1 of model image 3 = (8,8);

- $LC_4(x_1, x_1)$ from k_1 of model image 4 = (6,6);

the $AVG_{k_1}(x_1, x_1)$ of k_1 of the test image will be used as follows: $((3+7+8+6)/4, (3+7+8+6)/4) = (6,6)$.

When the AVG_{k_i} is calculated for each segment of the test image, each point in AVG_{k_i} is represented as a node in the face subgraph of test image. The edges between the adjacent nodes are fully connected. Furthermore, the Jet vector of each node in the probe image is also calculated as formulated in eq. (3). This process will be repeated for all modal images (which represent different individuals) in the database.

4.4. Recognition

After the face subgraph of probe image is constructed using AVG_{k_i} positions taken from particular modal images in the database, say I_j, the similarity between each node in the subgraph of reference image of the same modal images I_j and that of probe image is calculated using eq. 9. Then, the average similarity for all subgraph nodes in segment k_i is calculated as in Eq. (17).

$$SG_{k_i} = \frac{1}{M^2} \sum_{j=1}^{M^2} S_{k_i}(J_j, J'_j) \tag{17}$$

where M^2 is the number of nodes of the k_i face sub-graph and J_j is a jet of the reference image segment, J' is a jet of the probe image segment. The Overall average similarity of the entire image segments ($\boldsymbol{OS}$) is calculated as in Eq. (18).

$$OS = \frac{1}{2r} \sum_{i=1}^{2r} SG_{k_i} \tag{18}$$

Then the reference image that yields maximum overall average similarity with respect to the probe image is recognized as the target result. The overall average similarity for all reference images are sorted in descending order and then the reference image with the maximum similarity is addressed as rank one.

5. EXPERIMENTAL RESULTS AND DISCUSSIONS

In order to evaluate the effectiveness of the proposed method, two types of face image databases have been used: the AR [31] and FRGC ver2.0 [33]). A comprehensive experimental study has been carried out that takes into account face recognition under various situations including controlled/ideal condition, different lighting condition, different facial expressions, and partially occluded condition as done by other comparative methods [13, 23, 24, 18]. The AR database consists of over 4,000 frontal color images corresponding to 126 individuals (70 male and 56 female). Each individual subject is represented by 26 images taken in two separate sessions with two weeks time interval. Face images are subject to varying facial expressions (smile, anger, scream), illumination conditions (left light on, right light on and both lights on) and occlusions (sunglasses and scarf). The face images of 100 subjects (50 male and 50 female) including all variations were used in our experiments. In all the experiments conducted, face images were enhanced and normalized with standard preprocessing techniques (i.e., Median Filtering and Histogram Equalization) and then cropped. The resolution of the preprocessed and cropped images are 165 ×120 pixels. Fig. 10 shows samples of cropped faces from AR database.

The FRGC ver2.0 database contains 50,000 images distributed to training and validation sets. The training set consists of 12,776 images from 222 persons (individuals). The validation set contains images from 466 individuals collected in 4,007 sessions. The number of sessions used for taking photos of each person is different, ranging from 1 to 22 sessions (410 persons were photographed in two or more sessions). In each session, four controlled still images, two uncontrolled still images and one 3D scan were recorded. In all the experiments, the facial regions were cropped to a size of 160 × 160 pixels for recognition. In our experiments, all the 466 individuals in the validation set were used for testing. The first image in the first session was used as the reference image of the individual. One probe image per person was randomly selected from the remaining images of the person in all sessions.

The performance of the proposed method is compared with six benchmark approaches as abbreviated in Table. 1.

It is worth mentioning that the AR Face database has been used to evaluate the system performance on real occluded faces, variations in illumination and different expressions while the FRGC ver2.0 database has been employed to investigate the sensitivity of the proposed approach in the presence of synthetic occlusions of varying size.

We initialized the values of HCO-EBGM parameters as follow: HMCR=0.9 , PAR = 0.3, bw=0.01, and MI= 500. It has to be noted that the proposed HSO-EBGM runs 30 replication times for all experiments performed in the sections below and the recognition rates in the tables that follow (table 2 to table 5) refers to the average recognition rate.

5.1. The effect of number of segments on the performance of HSO-EBGM

In this section the AR face image databases are used to measure the impact of the face segments number $2r$ per face pertaining to the performance of the proposed HSO-EBGM approach. Experiments with two ($r = 1$), four and six face segments are performed as shown in Fig. 11. In the first experiment, the reference and model images are divided into two segments and then the optimal landmarks are generated for the model image in order to find the average landmarks using HSO-EBGM. In the second and third experiments, the image is divided into four ($r = 2$) and six ($r = 3$) segments respectively. Fig. 12 shows the results of the three experiments. It can be seen that the performance improves with increased number of segments where

the best recognition rate is achieved with six segments. In a nutshell, the more the number of subgraphs, the better will be the performance of the HSO-EBGM. However, as further increasing the number of segments will involve much computation load. Therefore, the number of face subgraphs are chosen to be six for all the subsequent experiments. This experiment also conveys that the proposed component-based HSO-EBGM yields significant performance improvement.

5.2. Sensitivity analysis of HSO-EBGM to varying occlusion sizes

In order to evaluate the robustness of the proposed method against sensitivity to varying occlusion sizes (occlusion challenge) using the FRGC ver2.0 database, these experimental evaluations have been performed. In this experiment, we applied the same experimental policy as in [13] on the large FRGC ver2.0 database. The probe images used in Section 4.3.1 were occluded by a square of s $\times$ s pixels at a random location, while the reference images remained unchanged without occlusion (as shown in Fig. 13). The size of the occlusion blocks has been varied from s = 10 (occlusion content of 0.39% within face image) up to s = 100 (39.06% occlusion content) with a step size of 10. The recognition rates of the proposed method and the other comparative approaches are plotted against the occlusion size in Fig. 14. It can be seen from Fig. 14 that the recognition rate of the proposed HSO-EBGM method remains more or less same against occlusion blocks which vary in size from 10×10 up to 40×40 pixels.

The performance of HSO-EBGM significantly outperform the EBGM and it stands next to the ESM approach against the occlusion challenge, while the recognition rate of other benchmark algorithms degraded. With a block size 100×100, the proposed method yielded a recognition rate of 43% compared to AWPPZMA and LEM where their recognition rates dropped significantly around 5%. In other words, the proposed approach is about *8 times* better than AWPPZMA and LEM in recognizing occluded faces. These results demonstrate the robustness of the proposed method in handling partial occlusions.

5.3. Face recognition under controlled /Ideal conditions

Here, we evaluate our proposed HSO-EBGM approach under relatively controlled conditions on both AR and FRGC ver2.0 databases. The recognition rate of HSO-EBGM was compared with those of ESM, AWPPZMA, LEM and EBGM as portrayed in Table 2. The best recognition rate is highlighted in **bold** (higher is better). In this experiment, the neutral faces taken in session one are chosen as references and the neutral faces taken in session two are chosen as the probe images. From Table 2, it can be seen that the HSO-EBGM outperform the EBGM and it showed comparable recognition performance on par with ESM, AWPPZMA and LEM methods on the AR database. However, the proposed method achieves lower recognition rate than ESM and similar recognition rate to AWPPZMA on the FRGC ver2.0 while it significantly outperformed the LEM method. This could be due to challenging large variations of the images for the same person in the FRGC ver2.0 database.

5.4. Face recognition experiment with realistic partial occlusions

In this experiment, the neutral image [Fig. 10 (a)] is used as a reference image while four occluded faces with sunglasses and scarf from both sessions [Fig. 10 (h-k)] are used for testing extracted from AR database. The recognition rates of the proposed method together with EBGM ,ESM, PISMA, and AWSGA approaches are summarized in Table 3. The best recognition rate is highlighted in **bold** (higher is better). Furthermore, Fig. 15 (a), (b), (c) and (d) show the recognition rates of our proposed HSO-EBGM approach compared with PISIMA and AWSGA on sunglasses and scarf of sessions 1 and 2 respectively. It is found that the occlusions affects the performance of all benchmark algorithms where the recognition rates drop ranging from 5.9% to 9.4% and 14.1% to 20.51% for faces with sunglasses with respect to session 1 and 2. It can be seen from Table 3 that the proposed approach achieves an average recognition rate comparable to ESM which is one of the standard algorithms to handle partial occlusion and significantly outperform the EBGM. Fig. 15 shows that the HSO-EBGM outperforms PISMA and AWSGA (about 20% to 30% significantly better) for all conditions in both sessions. These results justifies the ability of the proposed method to handle partial occlusions and further convinces that the proposed HSO-EBGM approach is capable of finding the optimal landmarks without requiring any prior knowledge or assumption of the occlusions and hence able to recognize faces which are prone to occlusions.

5.5. Face recognition challenge under facial expression variations

Variations caused by facial expression are among the common vital factors that could degrade the performance of a face recognition system. To evaluate the effect of different facial expressions (smiling, angry, and screaming Fig. 16) on the proposed HSO-EBGM performance, a dedicated experiment has been conducted using the AR database. Faces with neutral expression in the first session (recall Fig. 10 (a)) have been used as reference images; the face images with three different expressions (e.g., Fig. 16 (a), (b) and (c)) taken in the same session have been used as the test images. The experimental results are summarized in Table 4. The best recognition rate is highlighted in **bold** (higher is better). According to these results, it can be noted that only for the scream expression the recognition rates dropped for the proposed HSO-EBGM to 41%. However, better recognition accuracies have been observed for the smiling and the angry expressions. It can be observed that the scream expression has a more impact on the recognition accuracy than soft expressions such as smile and anger as revealed by our results. It is found that the proposed method significantly outperforms the ESM method under screaming expression and the LEM under smiling and angry expression variations. This is because the expression variation do not affect all local parts equally. As a result the proposed method which is basically a component-based approach achieved better recognition rate. Also, it can be noted that the recognition rate for anger expression merely increases by 0.9% compared to the neutral expression as shown in Table 2. This is because the test images and reference images were captured in the same session while the test images used in Section 5.3 were captured in the second session where the intra-class variations get increased when taking the session 2 pictures after a two week time interval. Fig. 17 shows the recognition rate of the proposed method in terms of Cumulative Match Characteristics (CMS) curve.

5.6. Face recognition under the illumination challenge

Illumination is one of the potential challenges encountered in the evaluation of any face recognition system. In this experiment, the sensitivity of the proposed approach with respect to illumination changes is evaluated. The neutral face images in the AR database taken in the first session (e.g. Fig. 10 (a)) were chosen as a single reference image. The face images under three different lighting conditions (e.g. Fig. 18 (a), (b), and (c)) taken in the same session were used as test images. The recognition rate are tabulated in Table 5. It can be seen from Table 5 that the proposed method outperforms ESM, AWPPZMA and LEM (which is one of the best illumination insensitive methods) under different lighting conditions. Note that in Table 5, the best recognition rate is highlighted in **bold** (higher is better). As the proposed component-based approach deploys and exploits Gabor wavelet features in an optimal manner, a good recognition performance has been achieved. The recognition rate of the proposed method is plotted in Fig. 19 in terms of CMC graphs.

6. Conclusion

In this contribution we have proposed a novel method called HSO-EBGM to automatically select facial landmarks by enabling the classical EBGM face recognition technique with a harmony search based optimization strategy. A single neutral image has been chosen as the reference image and four other images with different variations were used as model images. Component level face sub-graphs have been modeled on the segmented facial components. The landmarks which achieved maximum similarity between the sub-graphs of reference image segments corresponding to sub-graphs of model image segments ultimately represent the optimal landmarks. Empirically we have shown that such component-level facial sub-graphs have paved way for improved recognition rates. The proposed optimization mechanism allows the face recognition system to be fully automatic without relying on manual ground truth data to locate the landmarks. The overall similarity measure between two faces is computed by averaging the similarity entailed on their corresponding component-level partial face-graphs. Importantly, the proposed component-based optimization strategy enables the model to recognize occluded faces without requiring any prior knowledge or assumption about the occluded regions. Interestingly, the component-based mechanism deployed in the proposed HSO-EBGM for handling partial occlusions neither discard any occluded region from similarity calculation, nor reconstruct

this occluded region. The performance of the proposed approach is compared against the performance of recent state-of-the-art approaches using the AR and FRGC ver2.0 databases. The performance of HSO-EBGM stands next to the ESM approach against the occlusion challenge (face images occluded with random synthetic occlusion blocks of varying sizes), while the recognition rate of other benchmark algorithms degraded. With a block size of 100×100 pixels, the proposed method yielded a recognition rate of 43%compared to AWPPZMA and LEM where their recognition rates dropped significantly around 5%. In other words, the proposed approach is about *8 times* better than AWPPZMA and LEM in recognizing occluded faces bearing synthetic occlusions. When tested against real occlusions (faces occluded with sunglasses and scarf), the proposed HSO-EBGM approach achieved an average recognition rate comparable to ESM and about 20% to 30% respectively better than that of the recently proposed PISIMA and AWSGA occlusion models. Experimental results on recognizing faces by varying facial expressions justify the fact that the proposed method performed better than ESM, AWPPZMA and LEM approaches. Against the illumination challenge experiments, HSO-EBGM also yielded far better recognition accuracy when compared to these three state-art-of-the-art approaches. For future avenues, a good direction towards further improving recognition accuracy could be attained by investigating fusion models by integrating Gabor wavelets with other feature extraction techniques such as Histogram of Oriented Gradients (HOG), Local Binary Patterns (LBP) and so on. In our future work, we plan to extend the proposed optimization-based HSO-EBGM approach to model uncertainty elements inherent on other biometrics such as gait recognition.

7. Acknowledgements
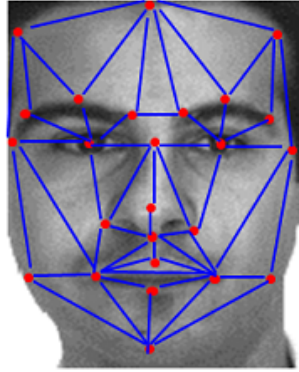
Figure 1: An example face-graph constructed from manually chosen fiducial points
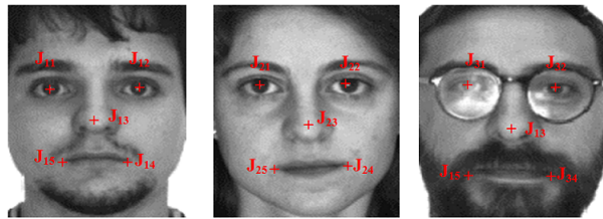
Figure 2: Manual Labeling

$$B_1 = \{J_{11}, J_{21}, J_{31}, \ldots\}$$
$$B_2 = \{J_{12}, J_{22}, J_{32}, \ldots\}$$
$$B_3 = \{J_{13}, J_{23}, J_{33}, \ldots\}$$
$$B_4 = \{J_{14}, J_{24}, J_{34}, \ldots\}$$
$$B_5 = \{J_{15}, J_{25}, J_{35}, \ldots\}$$

Figure 3: Bunch Graph construction

(x_1, x_1)

a

b
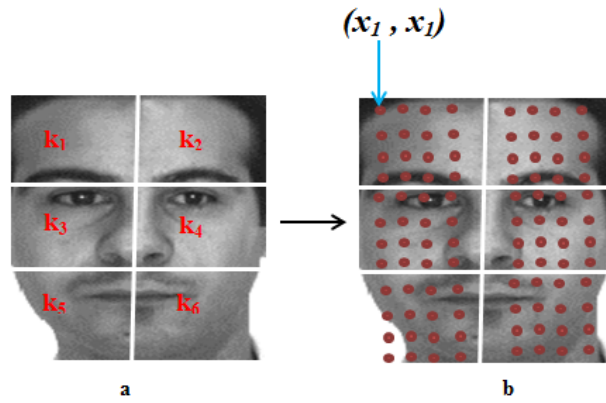
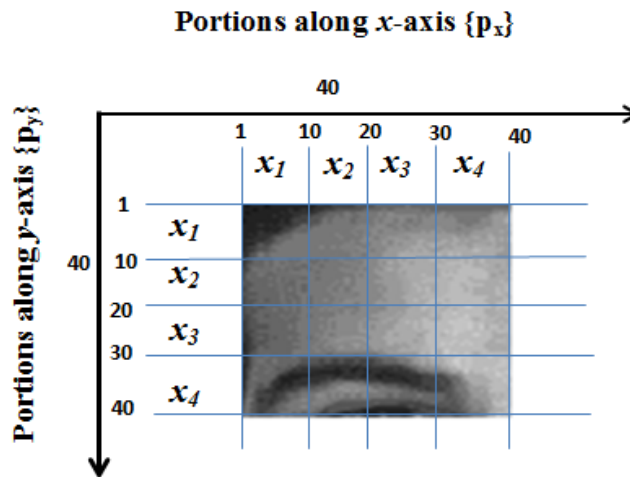Figure 4: Automatic formulation of facial landmarks for a typical segmented face image

Portions along x-axis $\{p_x\}$

Figure 5: An illustration that shows generation of landmarks for a typical face segment

14
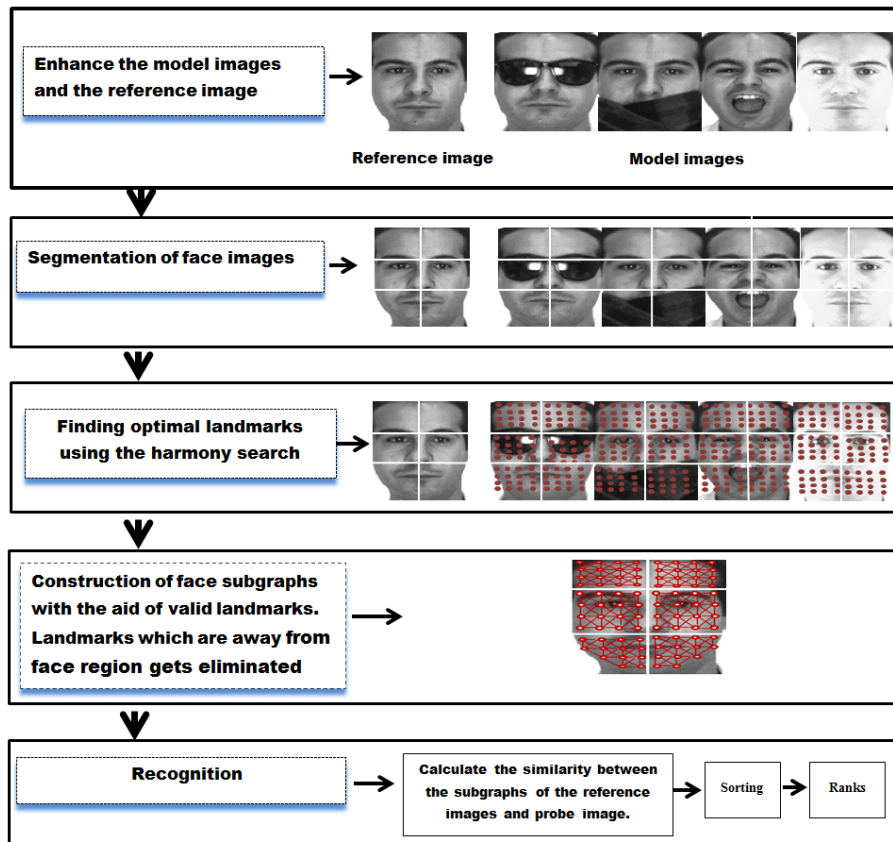
Figure 6: Framework of the proposed HSO-EMGM technique. This illustration use images taken from the AR face dataset. The diagram witnesses an instance of automatically generated face-subgraphs over a component-level segmented typical face image.
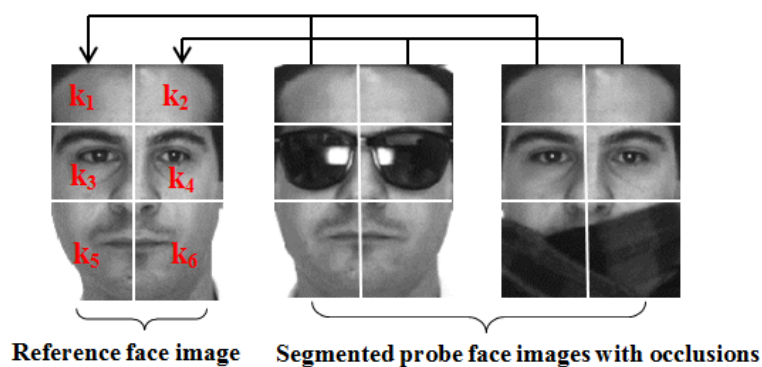
Figure 7: The proposed matching process. Basically the recognition process involves matching face sub-graphs of probe faces with that of reference face images.
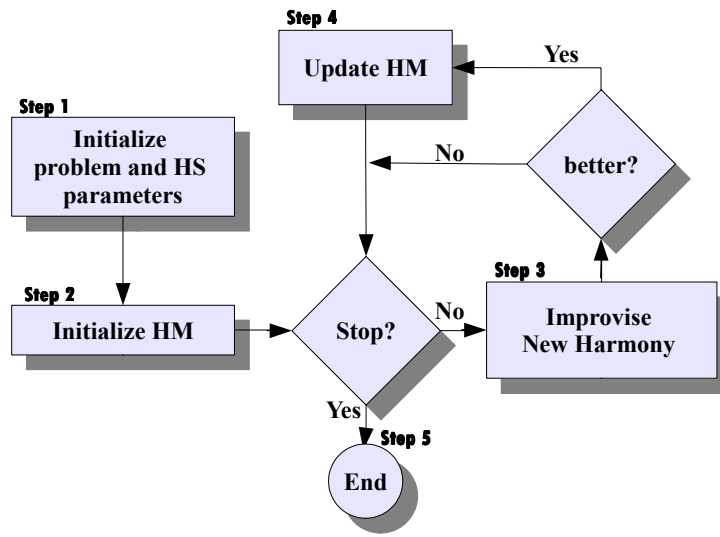
Figure 8: The Flowchart of the HS algorithm [4]

a. Before validation   b. After validation
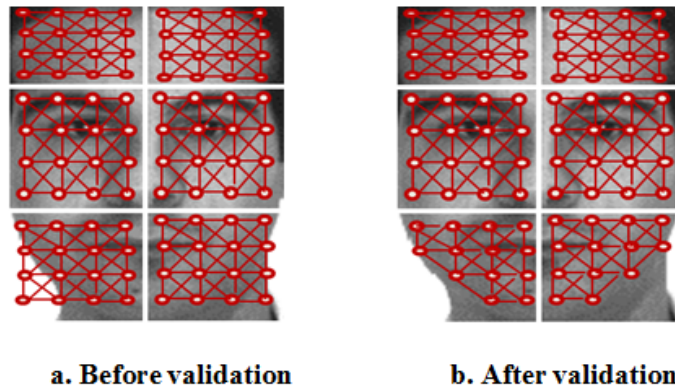
Figure 9: A validation scheme that ensures that landmarks are located within the face image
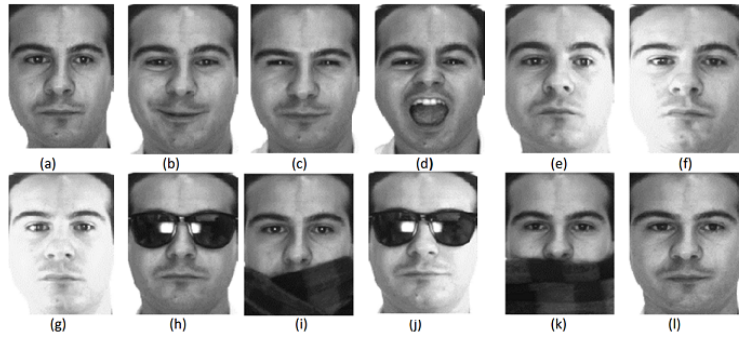
Figure 10: Instances of AR cropped face images for one subject. (a) Neutral face under controlled conditions taken in the session 1; (b-d) faces with smile,anger and scream expressions taken in the session 1; (e-g) faces under varying light conditions taken in the session 1; (h,i) partial occluded faces with sunglasses and scarf taken in the session 1; (j,k) partial occluded faces with sunglasses and scarf taken in the session 2; (l) neutral face under controlled conditions taken in the session 2

Figure 11: A typical face image being segmented to two, four and six segments
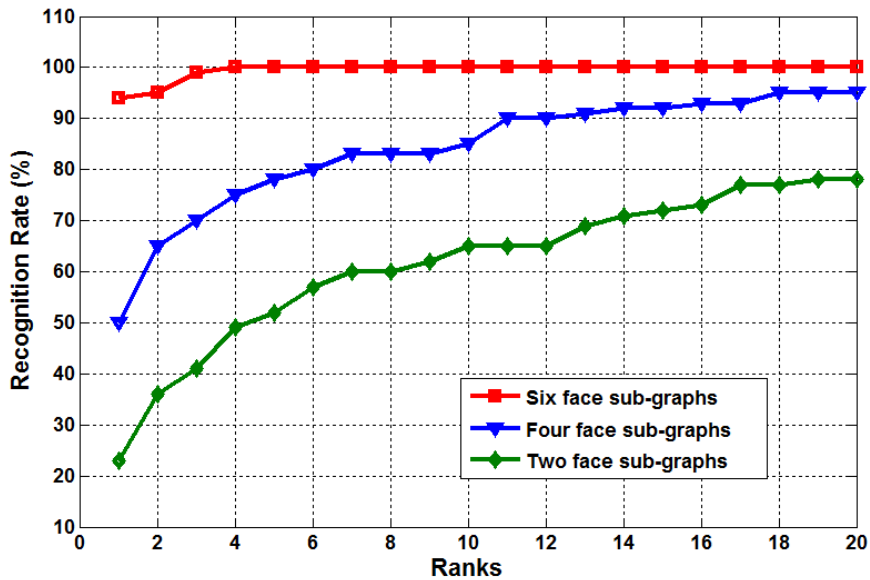
Figure 12: Comparison on the effect of varying the number of face sub-graphs

17

Figure 13: A typical face images being occluded with random occlusion blocks ranging from 10 × 10, 20 × 20, · · · , 100 × 100 respectively.
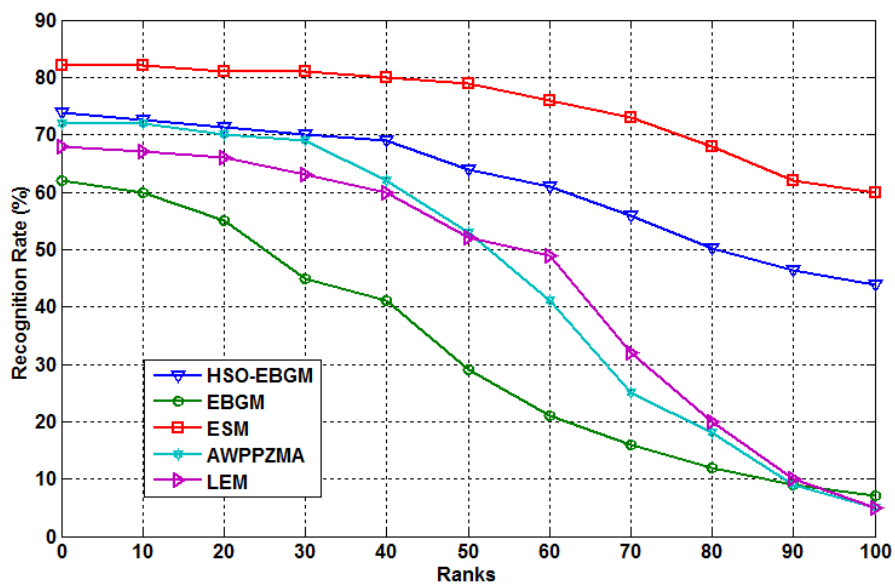

Figure 14: Recognition rate observed under varying sizes of random occlusion. Occlusions were gradually increased from 10 × 10, 20 × 20, . . . , 100 × 100.
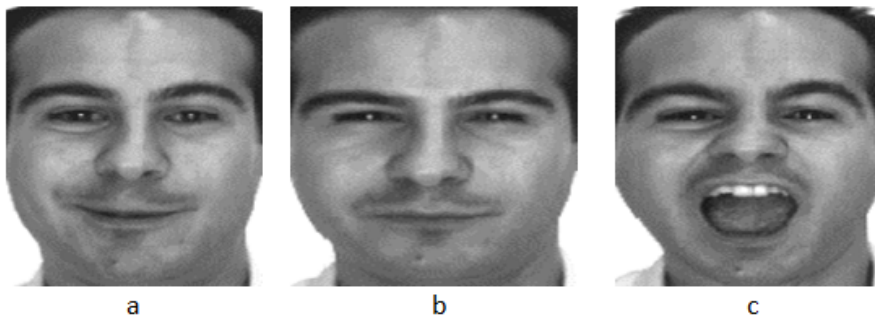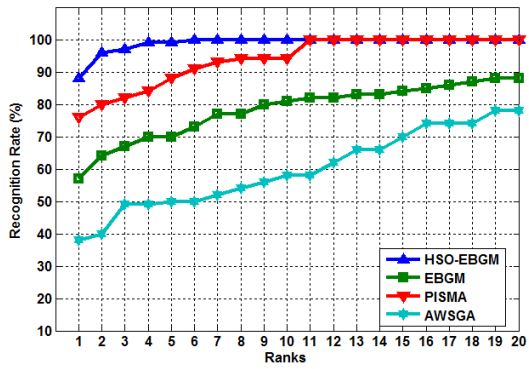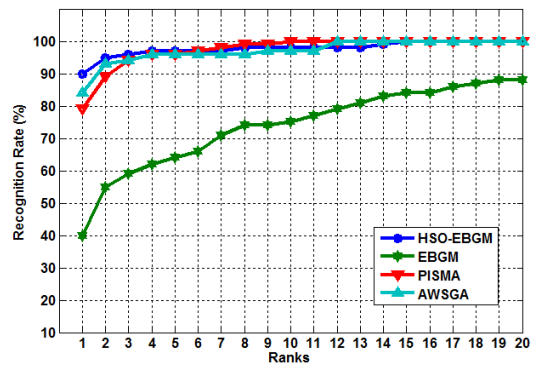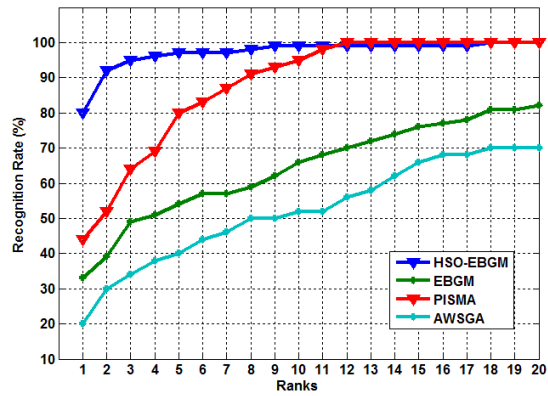

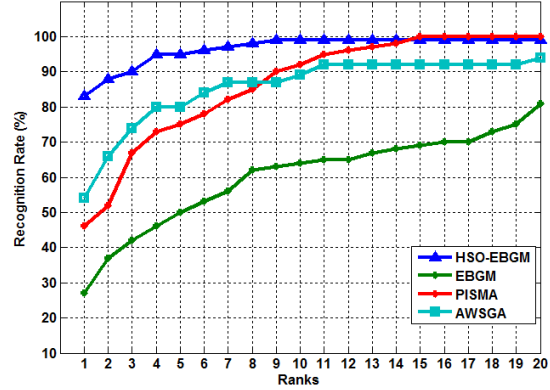Figure 16: Faces with different facial expressions: a. smiling, b. anger and c. scream .

18

(a) Sunglasses Session 1

(b) Scarf Session 1

(c) Sunglasses Session 2

(d) Scarf Session 2

Figure 15: Comparison of HSO-EBGM with PISIMA and AWSGA against realistic occlusions using the AR dataset in terms of Cumulative Match Characteristic(CMC) graphs.
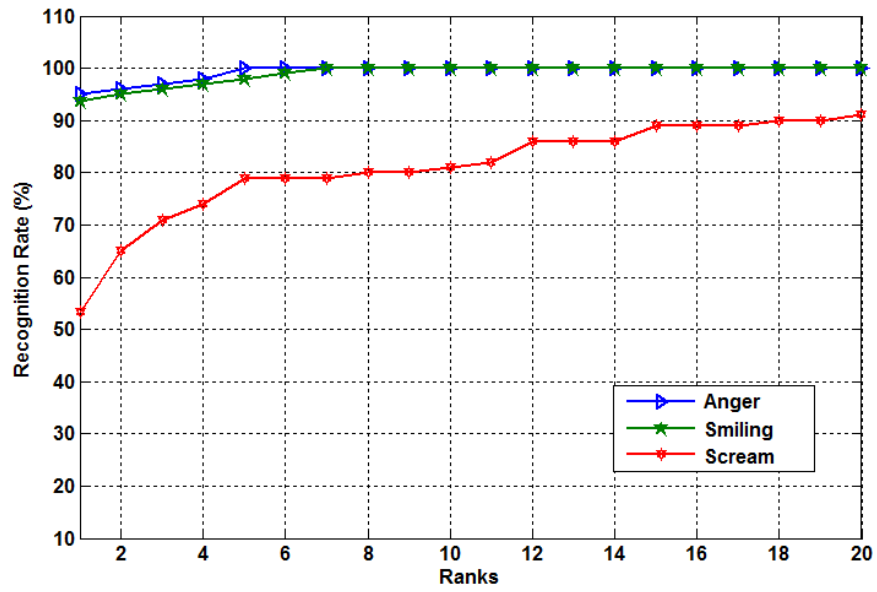
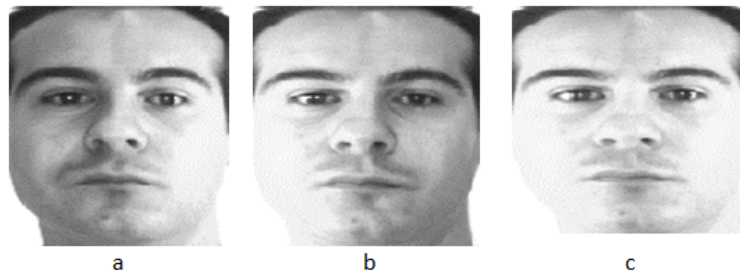Figure 17: Recognition rates obtained under different facial expressions.

Figure 18: Faces under different lighting conditions: a. left light on, b. right light on and c. both lights on.
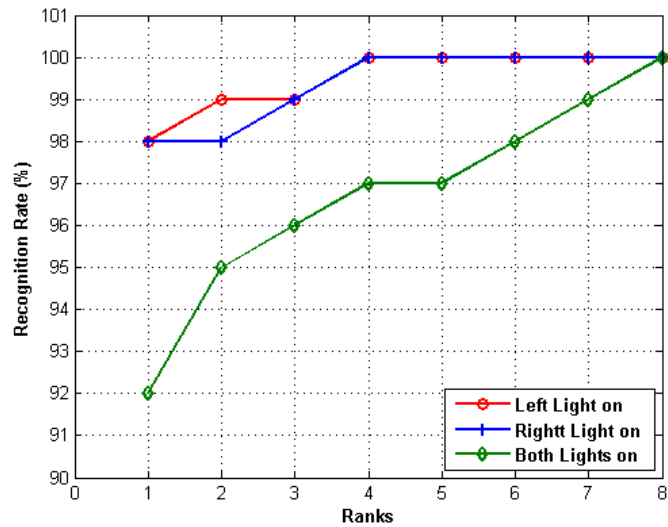
Figure 19: Recognition rates obtained under varying lighting conditions.

Table 1: Keys to the comparative methods

Key	Comparative method	Reference
EBGM	Elastic Bunch Graph Matching	[11]
PISMA	Psychophysically Inspired Similarity MApping	[38]
ESM	Ensemble String Matching	[13]
AWSGA	Adaptively Weighted Sub-Gabor Array	[23]
AWPPZMA	Adaptively Weighted Patch Pseudo Zernike Moment Array	[24]
LEM	Line Edge Map	[18]

Table 2: Comparative performance: Controlled/Ideal conditions

Methods	Recognition Rate	
	AR	FRGC
HSO-EBGM	94.1%	73.75 %
EBGM	84 %	61.42 %
ESM	**96.58** %	**82.62** %
AWPPZMA	92.31 %	72.75 %
LEM	**96.58** %	66.95 %

Table 3: Comparative performance: Real occlusions

| Methods | Recognition rate | | | | Average recognition rate |
| | Session-1 | | Session-2 | | |
	Sunglasses	Scarf	Sunglasses	Scarf	
HSO-EBGM	**88.20**%	91.8%	**80**%	83.3%	85.83%
EBGM	57 %	40%	33%	27%	36 %
ESM	87.18%	**94.87**%	76.07%	**88.3**%	**86.54**%
PISMA	78%	79%	55 %	49%	65.75%
AWSGA	38 %	84%	20%	70%	53 %

Table 4: Experimental results under varying facial expressions

| Methods | Recognition Rate | | | |
	Smiling	Anger	Scream	Average
HSO-EBGM	93.6%	**95**%	**53.4**%	**80.7**%
EBGM	74%	88%	29%	63.7 %
ESM	85.47%	87.18%	26.49%	72.36 %
AWPPZMA	**96.58**%	87.18%	38.46%	74.7%
LEM	79.49%	93.16%	31.62%	68.09 %
AWSGA	95.72%	94.87%	33.33%	74.64 %

Table 5: Experimental results under varying lighting conditions

| Methods | Recognition Rate | | | |
	Left light on	Right light on	Both lights on	Average
HSO-EBGM	**98.6** %	**98.3** %	**93**%	**96.63**%
EBGM	93%	89%	78%	86%
ESM	94.02%	94.02%	73.5%	87.18%
AWPPZMA	74.36%	64.96%	42.74%	60.69%
LEM	92.31%	91.45%	73.50%	85.75%
AWSGA	23.93%	5.98%	23.8%	17.9%

References

[1] Abdullah, M. F. A., Sayeed, M. S., Muthu, K. S., Bashier, H. K., Azman, A., & Ibrahim, S. Z. (2014). Face recognition with symmetric local graph structure (slgs). *Expert Systems with Applications*, *41*, 6131–6137.

[2] Abdulrahman, M., Gwadabe, T. R., Abdu, F. J., & Eleyan, A. (2014). Gabor wavelet transform based facial expression recognition using pca and lbp. In *Signal Processing and Communications Applications Conference (SIU), 2014 22nd* (pp. 2265–2268). IEEE.

[3] Abual-Rub, M. S., Al-Betar, M. A., Abdullah, R., & Khader, A. T. (2012). A hybrid harmony search algorithm for ab initio protein tertiary structure prediction. *Network Modeling Analysis in Health Informatics and Bioinformatics*, *1*, 69–85.

[4] Al-Betar, M. A., Doush, I. A., Khader, A. T., & Awadallah, M. A. (2012). Novel selection schemes for harmony search. *Applied Mathematics and Computation*, *218*, 6095–6117.

[5] Al-Betar, M. A., & Khader, A. T. (2012). A harmony search algorithm for university course timetabling. *Annals OR*, *194*, 3–31.

[6] Al-Betar, M. A., Khader, A. T., & Doush, I. A. (2014). Memetic techniques for examination timetabling. *Annals OR*, *218*, 23–50.

[7] Al-Betar, M. A., Khader, A. T., & Zaman, M. (2012). University course timetabling using a hybrid harmony search metaheuristic algorithm. *IEEE Transactions on Systems, Man, and Cybernetics, Part C: Applications and Reviews*, *42*, 664 – 681.

[8] Alia, O., & Mandava, R. (2011). The variants of the harmony search algorithm: an overview. *Artificial Intelligence Review*, *36*, 49–68.

[9] Alkareem, Y. A. Z. A., Venkat, I., Al-Betar, M. A., & Khader, A. T. (2012). Edge preserving image enhancement via harmony search algorithm. In *4th Conference on Data Mining and Optimization, DMO 2012, Langkawi, Malaysia, September 2-4, 2012* (pp. 47–52). URL: http://dx.doi.org/10.1109/DMO.2012.6329797. doi:10.1109/DMO.2012.6329797.

[10] Azeem, A., Sharif, M., Raza, M., & Murtaza, M. (2014). A survey: face recognition techniques under partial occlusion. *Int. Arab J. Inf. Technol.*, *11*, 1–10.

[11] Bolme., D. S. (2003). *THESIS ON ELASTIC BUNCH GRAPH MATCHING*. Master's thesis Colorado State University Fort Collins.

[12] Borgi, M. A., Labate, D., El Arbi, M., & Amar, C. B. (2015). Sparse multi-stage regularized feature learning for robust face recognition. *Expert Systems with Applications*, *42*, 269–279.

[13] Chen, W., & Gao, Y. (2013). Face recognition using ensemble string matching. *Image Processing, IEEE Transactions on*, *22*, 4798–4808.

[14] Deng, Y., Dai, Q., & Zhang, Z. (2011). Graph laplace for occluded face completion and recognition. *Image Processing, IEEE Transactions on*, *20*, 2329–2338. doi:10.1109/TIP.2011.2109729.

[15] Ekenel, H. m., & Stiefelhagen, R. (2009). Why is facial occlusion a challenging problem?, . *5558*, 299–308.

[16] Ensari, T., Chorowski, J., & Zurada, J. (2012). Occluded face recognition using correntropy-based nonnegative matrix factorization. In *Machine Learning and Applications (ICMLA), 2012 11th International Conference on* (pp. 606–609). volume 1. doi:10.1109/ICMLA.2012.112.

[17] Gao, J.-q., Fan, L.-y., & Xu, L.-z. (2013). Median null (sw)-based method for face feature recognition. *Applied Mathematics and Computation*, *219*, 6410–6419.

[18] Gao, Y., & Leung, M. K. (2002). Face recognition using line edge map. *Pattern Analysis and Machine Intelligence, IEEE Transactions on*, *24*, 764–779.

[19] Geem, Z. W. (2007). Optimal scheduling of multiple dam system using harmony search algorithm. In *Computational and Ambient Intelligence* (pp. 316–323). Springer.

[20] Geem, Z. W. (2008). Novel derivative of harmony search algorithm for discrete design variables. *Applied Mathematics and Computation*, *199*, 223 – 230.

[21] Geem, Z. W., Kim, J. H., & Loganathan, G. (2001). A new heuristic optimization algorithm: harmony search. *Simulation*, *76*, 60–68.

[22] Gonzalez, R. C., & Woods, R. E. (2002). Digital image processing. Prentice Hall.

[23] Kanan, H. R., & Faez, K. (2010). Recognizing faces using adaptively weighted sub-gabor array from a single sample image per enrolled subject. *Image and Vision Computing*, *28*, 438–448.

[24] Kanan, H. R., Faez, K., & Gao, Y. (2008). Face recognition using adaptively weighted patch pzm array from a single exemplar image per person. *Pattern Recognition*, *41*, 3799–3812.

[25] Kumar, D. et al. (2011). Harmony search algorithm for feature selection in face recognition. In *Computational Intelligence and Information Technology* (pp. 554–559). Springer.

[26] Lades, M., Vorbruggen, J., Buhmann, J., Lange, J., Von Der Malsburg, C., Wurtz, R., & Konen, W. (1993). Distortion invariant object recognition in the dynamic link architecture. *Computers, IEEE Transactions on*, *42*, 300–311. doi:10.1109/12.210173.

[27] Lee, K., & Geem, Z. (2004). A new structural optimization method based on the harmony search algorithm. *COMPUTERS & STRUCTURES*, *82*, 781–798. doi:10.1016/j.compstruc.2004.01.002.

[28] Li, X. X., Dai, D. Q., Zhang, X. F., & Ren, C. X. (2013). Structured sparse error coding for face recognition with occlusion. *Image Processing, IEEE Transactions on*, *22*, 1889–1900. doi:10.1109/TIP.2013.2237920.

[29] Manjarres, D., Landa-Torres, I., Gil-Lopez, S., Del Ser, J., Bilbao, M., Salcedo-Sanz, S., & Geem, Z. (2013). A survey on applications of the harmony search algorithm. *Engineering Applications of Artificial Intelligence*, *26*, 1818–1831.

[30] Martinez, A. M. (2002). Recognizing imprecisely localized, partially occluded, and expression variant faces from

a single sample per class. *Pattern Analysis and Machine Intelligence, IEEE Transactions on*, *24*, 748–763. doi:10.1109/TPAMI.2002.1008382.

[31] Martinez, A. M., & Benavente, R. (1998). *"The AR face database"*. Tech. Rep. 24,.

[32] Min, R., Hadid, A., & Dugelay, J. (2011). Improving the recognition of faces occluded by facial accessories, . (pp. 442–447).

[33] Phillips, P. J., Flynn, P. J., Scruggs, T., Bowyer, K. W., Chang, J., Hoffman, K., Marques, J., Min, J., & Worek, W. (2005). Overview of the face recognition grand challenge. In *Computer vision and pattern recognition, 2005. CVPR 2005. IEEE computer society conference on* (pp. 947–954). IEEE volume 1.

[34] Phillips, P. J., Moon, H., Rizvi, S., Rauss, P. J. et al. (2000). The feret evaluation methodology for face-recognition algorithms. *Pattern Analysis and Machine Intelligence, IEEE Transactions on*, *22*, 1090–1104.

[35] Sawalha, R., & Doush, I. A. (2012). Face recognition using harmony search-based selected features. *International Journal of Hybrid Information Technology*, *5*, 1–16.

[36] Senaratne, R., Halgamuge, S., & Hsu, A. (2009). Face recognition by extending elastic bunch graph matching with particle swarm optimization. *Journal of Multimedia*, *4*, 204–214.

[37] Sinha, P., Balas, B., Ostrovsky, Y., & Russell, R. (2006). Face recognition by humans: Nineteen results all computer vision researchers should know about. *Proceedings of the IEEE*, *94*, 1948–1962.

[38] Venkat, I., Khader, A. T., Subramanian, K., & Wilde, P. D. (2013). Recognizing occluded faces by exploiting psychophysically inspired similarity maps. *Pattern Recognition Letters*, *34*, 903 – 911.

[39] Wei, X., Li, C.-T., Lei, Z., Yi, D., & Li, S. Z. (2014). Dynamic image-to-class warping for occluded face recognition. *Information Forensics and Security, IEEE Transactions on*, *9*, 2035–2050.

[40] Wiskott, L., Fellous, J.-M., Kuiger, N., & Von der Malsburg, C. (1997). Face recognition by elastic bunch graph matching. *Pattern Analysis and Machine Intelligence, IEEE Transactions on*, *19*, 775–779. doi:10.1109/34.598235.

[41] Wright, J., Yang, A., Ganesh, A., Sastry, S., & Ma, Y. (2009). Robust face recognition via sparse representation. *Pattern Analysis and Machine Intelligence, IEEE Transactions on*, *31*, 210–227. doi:10.1109/TPAMI.2008.79.

[42] Xiaorong, P., Zhihu, Z., Heng, T., & Tai, L. (2012). Partially occluded face recognition using subface hidden markov models. In *Computing and Convergence Technology (ICCCT), 2012 7th International Conference on* (pp. 720–725).

[43] Yan, H., Wang, P., Chen, W., & Liu, J. (2015). Face recognition based on gabor wavelet transform and modular 2dpca, .

[44] Yang, A., Zhou, Z., Balasubramanian, A., Sastry, S., & Ma, Y. (2013). Fast ℓ_1- minimization algorithms for robust face recognition. *Image Processing, IEEE Transactions on*, *22*, 3234–3246.

[45] Zhao, Y., Liu, Y., Liu, Y., Zhong, S., & Hua, K. A. (2015). Face recognition from a single registered image for conference socializing. *Expert Systems with Applications*, *42*, 973–979.